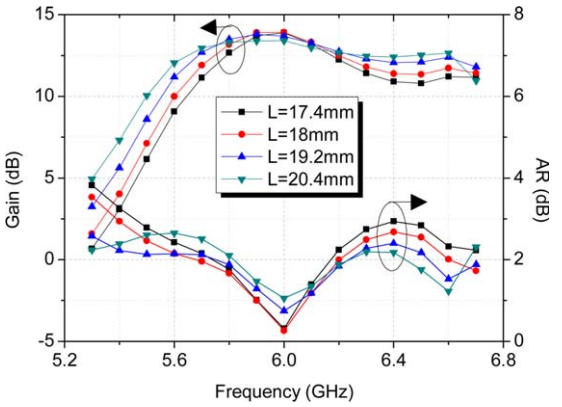

Figure 16 Simulated ARs and broadside gains of the proposed antenna with different *L*. [Color figure can be viewed in the online issue, which is available at wileyonlinelibrary.com]

and measured patterns in $\varphi = 45°$ plane at 5.6, 5.8, 6.2, and 6.5 GHz are shown in Figure 10, respectively. The measurements agree well with simulations along main beams, and the side lobe is below −13 dB in the whole operating frequency band. Moreover, low cross-polarization in the main beam is achieved in the low frequency but high in the high frequency.

4. PARAMETRIC STUDIES

To understand how the dimensions influence the antenna performances, parametric studies are performed by HFSS™. First, we focus on the square patches of the HIS structures with a width a, in this research $a + g = 5$ mm is fixed. Simulated ARs and broadside gains of the proposed antenna at 6 GHz versus different a are shown in Figure 11. Figure 12 shows the simulated ARs and broadside gains of the proposed antenna with different a will shift the operating frequency band downwards.

The total radiated electric field at the broadside direction propagation one time between two reflectors is shown as follows:

$$\bar{E} = E_0\left(\vec{a} \cdot e^{-jkz-2jkd+j\theta-j\pi}\right)$$

where E_0 denotes the magnitude of electrical fields, k is the free-space wave number, d is the distance of two reflectors, and θ is the reflection phase of the ground plane.

In order to get a superimposed result,

$$-2kd+\theta-\pi = 2n\pi \quad n = 0, 1, 2....$$

When a increases, θ will be decreased. As

$$kd = \frac{2\pi d}{\lambda}$$

it is obvious that the operating frequency band is moved downward, which agree well with the results in Figure 12.

Second, we focus on the diameter of subreflector D_2, simulated ARs, and broadside gains of the proposed antenna at 6 GHz versus different D_2 are shown in Figure 13. Figure 14 shows the simulated ARs and broadside gains of the proposed antenna with different D_2. It can be seen that as D_2 increases, the minimum ARs are always kept at around 6 GHz and the gain is enlarged. Meanwhile, another issue arise that the gain decreased rapidly after maximum gain achieved, so the 3-dB gain bandwidth is reduced as shown in Figure 14.

At last, we focus on the length of the dipoles L. Simulated ARs and broadside gains of the proposed antenna at 6 GHz versus different L are shown in Figure 15. Figure 16 shows the simulated ARs and broadside gains of the proposed antenna with different L. It can be seen when the length of the dipoles L is changed, a maximum gain is achieved and the minimum ARs are always kept at around 6 GHz. However, the gain decreased rapidly when L goes beyond the optimum value, causing a narrower 3-dB gain.

5. CONCLUSION

A SBA is investigated in the article in which total height is reduced by using the HIS as a ground plane. It is excited by crossed dipoles through a power divider to radiate circular polarized wave. Acceptable agreement between simulations and measurements prove the validity of the simulations and the success of the design as a candidate for circular polarization applications and miniaturization. The antenna presents the 3-dB AR bandwidth of more than 25%, the 3-dB gain bandwidth of 22.5%, symmetrical radiation patterns, and the SWR is always below 2 in the operating frequency band. Meanwhile, the total height of the antenna can be reduced to only 0.3 λ_0, which is much smaller than a height of 0.6 λ_0 of normal SBA.

ACKNOWLEDGMENT

This work was supported by the National Natural Science Foundation of China (No. 61101036) and the Fundamental Research Funds for the Central Universities (No. ZYGX2010J028).

REFERENCES

1. P.F. Driessen, Gigabit/s indoor wireless systems with directional antennas, IEEE Trans Commun 44 (1996), 1034–1044.
2. H.W. Ehrenspeck, The short-backfire antenna, Proc IEEE 53 (1965), 1138–1140.
3. Y. Yamada, T. Takan, and N. Ishida, Compact antenna equipment for maritime satellite communication systems, Trans IECE 62-B (1979), 844–846.
4. K. Fujimoto and J.R. James, Mobile antenna systems handbook, 2nd ed., Artech House, Norwood, 2002, pp. 542–545.
5. A. Kumar and H.D. Hristov, Microwave cavity antennas, Artech House, Norwood, MA, 1989, pp. 215–387.
6. D. Sievenpiper, L. Zhang, and E. Yablonovitch, High-impedance electromagnetic ground planes, In: IEEE MTT-S International Microwave Symposium Digest, 1999, Anaheim, CA, pp. 1529–1532.
7. F. Yang and Y. Rahmat-Samii, Reflection phase characterizations of the EBG ground plane for low profile wire antenna applications, IEEE Trans Antennas Propag 51 (2003), 2691–2703.

DESIGN OF A CPW-FED C-SHAPED SLOT ARRAY ANTENNA FOR COAL MINE/TUNNEL APPLICATIONS

Yang Zhao, Zhijun Zhang, and Zhenghe Feng
State Key Lab of Microwave and Communications, Department of Electronic Engineering, Tsinghua University, Beijing 100084, China; Corresponding author: zjzh@tsinghua.edu.cn

Received 27 November 2012

ABSTRACT: *This article proposes a C-shaped slot array antenna for coal mine or tunnel communications fed by a coplanar waveguide slot line. Each antenna element has a short-ended C-shaped slot pair. Instead of working at the basic mode, in the way that traditional*

half-wavelength straight slots do, the proposed C-shaped slot pair of each element operates at the first high-order mode to realize maximum bidirectional radiation at boresight. The design procedure is generalized, and some influential parameters are studied. A four-element C-shaped slot array antenna sample is designed, fabricated, and measured. The measured impedance bandwidth for $|S_{11}| \leq -10$ dB is 230 MHz (2.37 GHz to 2.60 GHz), and the measured in-band maximum gains lie in the range of 9.0–11.1 dBi. The measured bidirectional radiation patterns remain stable without main beam tilting across the 2.4-GHz WLAN band. The measured and the simulated results show good agreement. © 2013 Wiley Periodicals, Inc. Microwave Opt Technol Lett 55:1784–1789, 2013;View this article online at wileyonlinelibrary.com. DOI 10.1002/mop.27695

Key words: *coplanar waveguide; slot array; bidirectional*

1. INTRODUCTION

Bidirectional radiation is usually required for coal mine or tunnel systems. The performance of the system is always degraded by severe signal attenuation inside the coal mine or tunnel channels where the dielectric constant or wall conductivity is relatively high. Meanwhile, severe multipath effects would be aroused by reflections from the side walls or diffractions from other objects. Therefore, antennas with high gains and bidirectional radiation patterns are urgently needed to combat the attenuation problem and multipath effects for stable and reliable coal mine or tunnel communications.

Slot-type radiators have bidirectional radiation, and they can be promising candidates for coal mine or tunnel wireless applications. The coplanar waveguide (CPW) feed line has also gained increasing popularity because it has many advantages in array design, such as lower radiation loss, less dispersion, and uniplanar structure, among others. Many researchers have studied CPW-fed slot array antennas [1–11]. A two-dimensional slot array antenna fed by a CPW is designed in [1], where a one-wavelength CPW slot transmission line is meandered between two half-wavelength-spaced adjacent elements to feed the elements in phase and realize high gains. A four-element slot array excited by a CPW is presented in [2], and mutual admittances between the slots are calculated based on a reciprocity theorem. An 11-element brick-wall array antenna fed by a CPW is introduced in [3] with high gain performances. A six-element horn-shaped slot array antenna fed by a CPW is proposed in [4] to obtain a wide impedance bandwidth and stable radiation characteristics. In [5], a three-element CPW-fed slot array antenna based on inductive coupling is presented. A CPW-based leaky-wave slot array antenna is proposed in [6], with element spacing far smaller than one wavelength for bidirectional radiation. An open-ended rampart slot array fed by a CPW is designed in [7] to get higher in-band peak gains than the short-ended counterpart. A CPW-fed log-periodic slot array is proposed in [9–11] to achieve wide-band performance.

In this article, we propose a slot array antenna with C-shaped elements for high-gain performance. The proposed antenna is fed by a CPW slot line and is printed on a substrate with a single metal layer. Thus, it is easily constructed. The proposed C-shaped slot element can be formed by bending the traditional half-wavelength straight slot twice. It is also much easier for the C-shaped slot element to construct an antenna array than it is for the traditional straight slots used in the literature, as in [1]. The reason for this is that a half-wavelength CPW slot feed line is enough to excite the adjacent C-shaped slot elements in phase, and thus eliminate the meandering of a one-wavelength slot line within a half-wavelength element separation. The pattern symmetry and antenna efficiency can be improved as well.

The article is organized as follows. In Section 2, we describe the geometry of the proposed array antenna and analyze the usable operating mode for maximum radiation at the boresight. In Section 3, we generalize the design procedure, study the influence of some of the important parameters, and compare the measured results of the designed prototype with the results of the simulated one.

2. ANTENNA DESIGN

2.1. Antenna Structure

Figure 1 shows the geometry of the proposed four-element C-shaped slot array antenna with bidirectional radiation patterns for coal mine or tunnel applications. The proposed antenna is designed on a single-layered F_4B dielectric substrate with a relative permittivity of $\varepsilon_r = 2.55$, a thickness of $h = 1.5$ mm, and a loss tangent of $\tan\delta = 0.005$.

The radiating element of the proposed array antenna is a C-shaped slot pair with a slot width of S_w and a total slot length of $S_l = 2 \times SL_1 + SL_2$, as indicated by the dashed circle in the upper right side of Figure 1. C_d stands for the spacing between the adjacent two elements, and the spacing is about half the

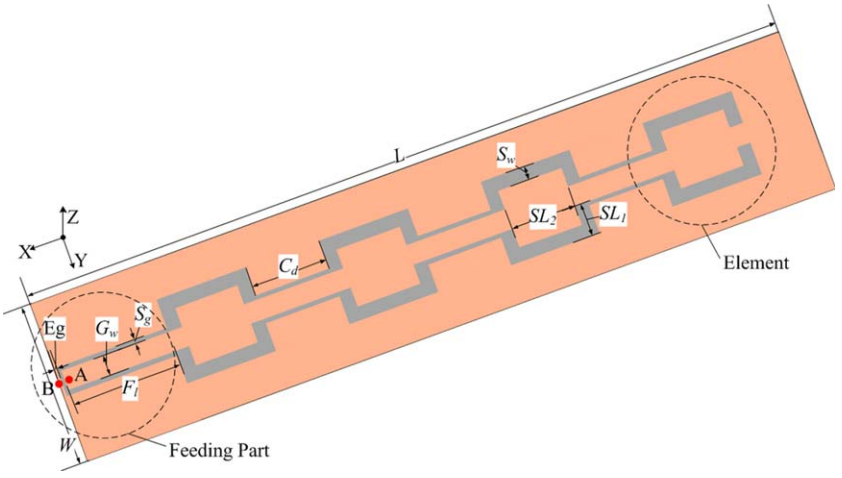

Figure 1 Geometry of the proposed C-shaped slot array antenna. [Color figure can be viewed in the online issue, which is available at wileyonlinelibrary.com]

TABLE 1 Dimensions of the Proposed Slot Array

Parameter	G_w	S_g	F_1	E_g	S_w	SL_1	SL_2	C_d	W	L
Value (mm)	10.0	4.0	67.0	2.0	8.0	18.0	50.0	42.0	100.0	500.0

guided wavelength $\lambda_g/2$ at resonance. A CPW with a single metalized dielectric layer feeds the C-shaped slot array antenna. For each element, a pair of C-shaped slots is etched symmetrically on the conducting plane of the CPW. G_w denotes the width of the CPW signal strip, S_g the gap distance between the signal strip and the coplanar ground is. F_1 indicates the feeding length of the CPW transmission line. The CPW coplanar ground is extended by a length of E_g for the easy installation of the exciting cable. A 50-Ω semi-grid coaxial cable is used to excite the mode of the CPW transmission line. The inner conductor of the cable is soldered to point A on the CPW signal strip, and the outer shield is connected to point B on the coplanar ground. Points A and B are marked by solid red pot, and the feeding part is enclosed by the dashed circle in the lower left side of Figure 1.

A four-element CPW-fed C-shaped slot array antenna is designed in the 2.4-GHz wireless local area network (WLAN) band centered at 2.44 GHz for underground coal mine or tunnel wireless communications. Table 1 lists the value of each parameter labeled in Figure 1.

2.2. Mode Analysis

The antenna is simulated and analyzed by Ansoft HFSS based on the finite element method. Figure 2 shows the instantaneous electrical field distributions for the basic mode and the first high-order mode of the proposed C-shaped slot element. The C-shaped slot pair can be viewed as a pair of the traditional straight slots etched perpendicular to the CPW slot line with two bends. Just as with the traditional straight slot element, the basic mode of the C-shaped slot element resonates at $\lambda_{g0}/2$, where λ_{g0} is the guided wavelength of the basic mode, and its resonant frequency F_b can be estimated by formula (1). For the basic mode, the electrical fields inside the slot have a half sinusoidal distribution with a maximum at the center of the slot SL_2 and two nulls at the end of the slot SL_1, as plotted in Figure 2(a).

The high-order mode resonates at λ_g, where λ_g is the guided wavelength of the high-order mode, and its resonant frequency F_h can be estimated by formula (2). For the first high-order mode, the electrical fields inside the slot have one entire sinusoidal distribution with a null at the center of slot length SL_2 and two nulls at the end of the slot SL_1, as plotted in Figure 2(b).

$$F_b = \frac{c}{2} \times \frac{1}{\sqrt{(\varepsilon_r + 1)/2}} \times \frac{1}{(2 \times SL_1 + SL_2)} \tag{1}$$

$$F_h = c \times \frac{1}{\sqrt{(\varepsilon_r + 1)/2}} \times \frac{1}{(2 \times SL_1 + SL_2)} \tag{2}$$

For the single radiating element, the C-shaped slot pair has opposite phases everywhere inside the slots at the basic resonating mode; a null will be produced at the boresight in the radiation pattern, which is not suitable for coal mine or tunnel communications. At the first high-order mode, however, a phase inversion is experienced in the center of slot SL_2, and thus the electrical fields of the two bent slots SL_1 will have the same phase state. Therefore, maximum gain can be obtained at the broadside boresight owing to the in-phase superposition of the first high-order electrical fields, and this is applicable to the coal mine or tunnel channels. We call the first high-order mode the operating mode.

Figure 3 shows the instantaneous electrical field distribution at resonance on the radiating slot of the designed four-element C-shaped slot array antenna operating at the first high-order mode. We can see that all the bent slots SL_1 in the slot pairs have the same phase state. Thus, high-gain bidirectional patterns with maximum gain at boresight can be produced. The proposed C-shaped slot array is *x*-polarized according to the coordinate axis shown in Figure 1.

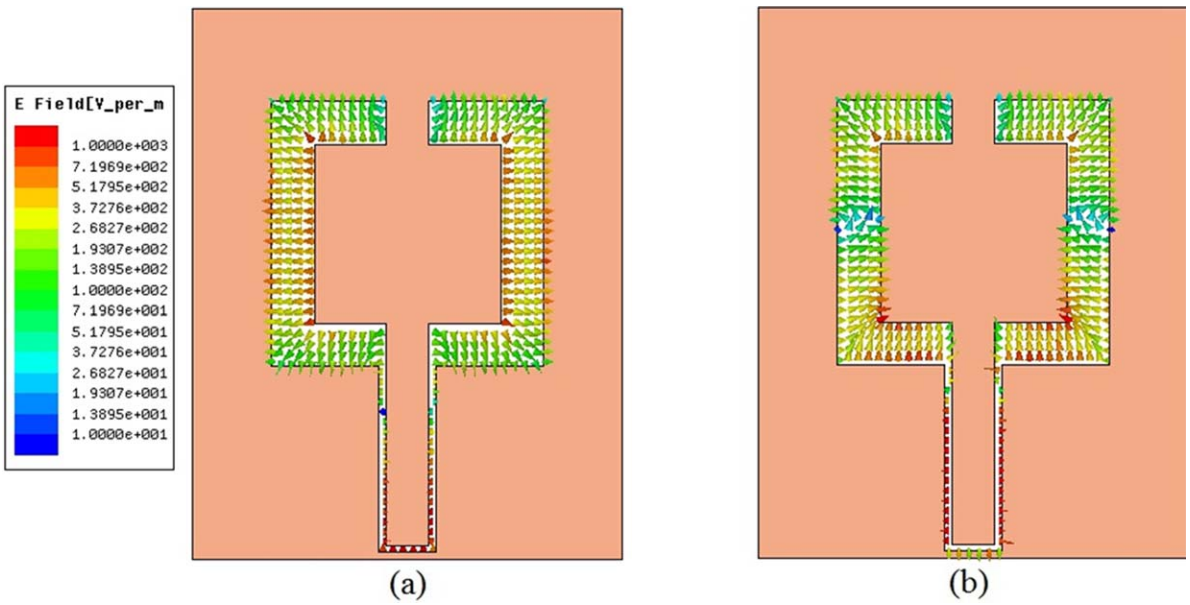

Figure 2 Instantaneous electrical field distributions at resonance on the proposed C-shaped slot element: (a) Basic mode; (b) First high-order mode. [Color figure can be viewed in the online issue, which is available at wileyonlinelibrary.com]

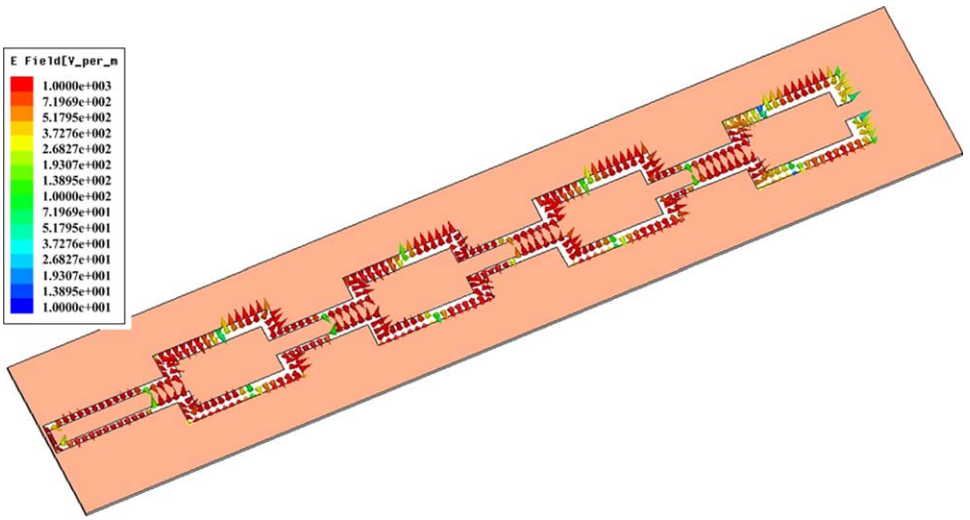

Figure 3 Instantaneous electrical field distributions at resonance on the radiating aperture of the four-element C-shaped slot array antenna. [Color figure can be viewed in the online issue, which is available at wileyonlinelibrary.com]

3. RESULTS AND DISCUSSION

3.1. Design Procedure

The proposed antenna has a simple uniplanar structure. We summarize the following procedure is to design a generalized CPW-fed C-shaped slot array antenna: (1) Calculate the total length S_1 of the C-shaped slot element to make it resonant at the first high-order mode based on the desired operating frequency. (2) Set up the element spacing C_d at about half the guided wavelength at resonance to make all the elements in phase excited by the CPW slot line. (3) Adjust the aspect ratio SL_1/SL_2 of the C-shaped slot element while keeping the total slot length S_1 fixed to about one guided wavelength at resonance to get maximum directivity. (4) Change the feeding length of the CPW transmission line F_1 and other parameters to make the antenna impedance matched at the resonant frequency. (5) Readjust the parameters to make the antenna both operating mode correct and impedance matched at the resonant frequency.

3.2. Parameter Study

We examine some important parameters that significantly influence the performance of the designed four-element C-shaped slot array antenna. The impedance matching and maximum gain are considered simultaneously when adjusting one of the parameters while keeping fixed all others listed in Table 1.

Figure 4 shows the simulated amplitude of the reflecting coefficient and the antenna gain with different lengths of SL_1 and SL_2 while keeping the total length S_1 fixed. The operating frequency band remains almost unchanged, but the impedance matching becomes worse when the slot length of SL_2 increases while SL_1 decreases. However, the antenna gain becomes higher for a longer slot length of SL_2. Therefore, a balance should be made between the impedance bandwidth and gain.

Figure 5 shows the influence of element spacing on the resonant frequency, the impedance bandwidth, and the antenna gain. The element spacing C_d controls the mutual coupling and thus affects the impedance matching to the feeding port and the radiation pattern. We can see from Figure 5 that both the resonant mode and the antenna gain will shift to higher frequency when the elements become closer.

Figure 6 shows the influence of the feeding length of the CPW transmission line. The length of the CPW feed line F_1 plays an important part in the antenna impedance matching but causes almost no change to the resonant mode.

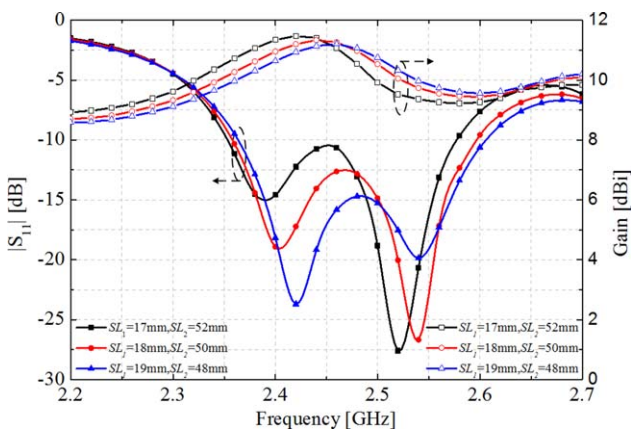

Figure 4 Simulated $|S_{11}|$ and gains of the proposed slot array antenna with different c-shapes while keeping fixed the total slot length $2 \times SL_1 + SL_2$ (Left: $|S_{11}|$, Right: Gain). [Color figure can be viewed in the online issue, which is available at wileyonlinelibrary.com]

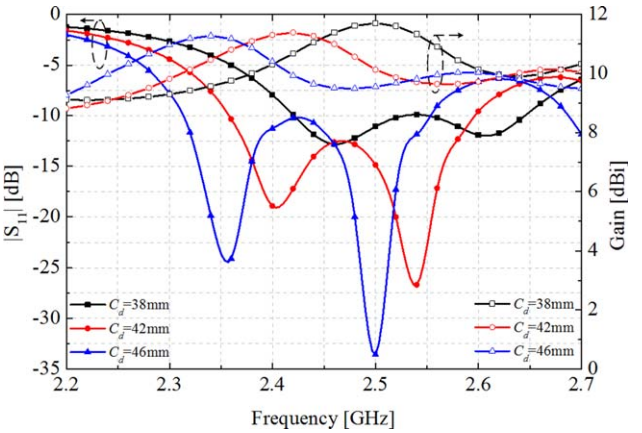

Figure 5 Simulated $|S_{11}|$ and gains of the proposed slot array antenna with different element distance C_d (Left: $|S_{11}|$, Right: Gain). [Color figure can be viewed in the online issue, which is available at wileyonlinelibrary.com]

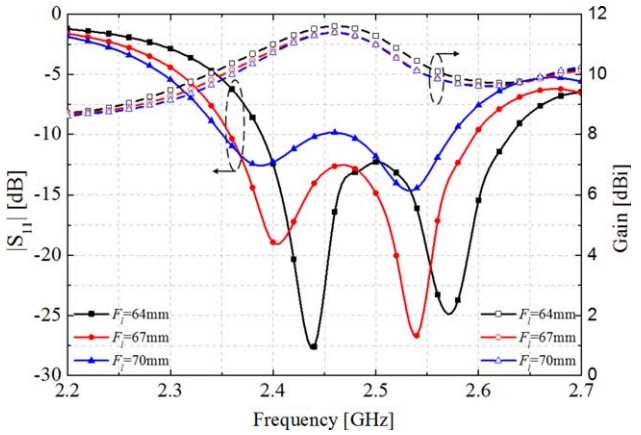

Figure 6 Simulated $|S_{11}|$ and gains of the proposed slot array antenna with different feeding length F_1 (Left: $|S_{11}|$, Right: Gain). [Color figure can be viewed in the online issue, which is available at wileyonlinelibrary.com]

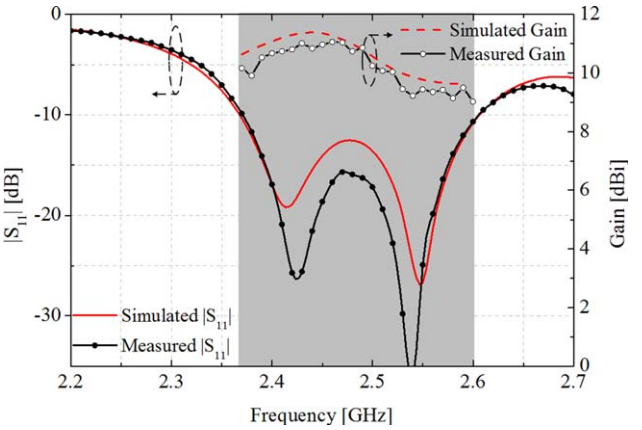

Figure 8 Measured and simulated $|S_{11}|$ and gain of the proposed antenna. [Color figure can be viewed in the online issue, which is available at wileyonlinelibrary.com]

3.3. Measurement and Discussion

The designed four-element C-shaped slot array sample for coal mine or tunnel 2.4-GHz WLAN communication is fabricated and measured. Figure 7 shows the sample. Figure 8 compares the measured and the simulated reflection coefficients and gain. The measured and the simulated impedance bandwidths for $|S_{11}| \leq -10$ dB are 230 MHz (2.37 GHz to 2.60GHz) and 230 MHz (2.37 GHz to 2.60 GHz), respectively. The simulated maximum gain is 11.4 dBi at 2.45 GHz and the measured maximum gain is 11.1 dBi at 2.46 GHz. The shadow region of Figure 8 shows the measured in-band maximum gain. A variation of about 2 dB is observed for the measured $|S_{11}| \leq -10$ dB regions. The radiation pattern in the 2.4-GHz WLAN band remains stable with almost no main beam tilting. Figure 9 shows the measured and the simulated normalized radiation patterns at 2.44 GHz, and they agree well with each other. The pattern in the *xoz* plane is narrower than that in the *yoz* plane. This is the result of one-dimensional array arranged in the *x*-axis direction. The measured and the simulated results show good agreement, and the discrepancies can be attributed to uncertainty of relative dielectric constant and dielectric loss, the manufacturing deviation, the measurement system set up, and so on.

4. CONCLUSION

This article presents a CPW-fed four-element C-shaped slot array antenna with bidirectional radiation pattern and high-gain performance for underground coal mine or tunnel communications. The antenna is printed on a single-layered substrate with a one-side metalization. The proposed antenna has a uniplanar and symmetrical structure and can be easily fabricated. The operating modes are analyzed and the generalized design procedure is provided. The

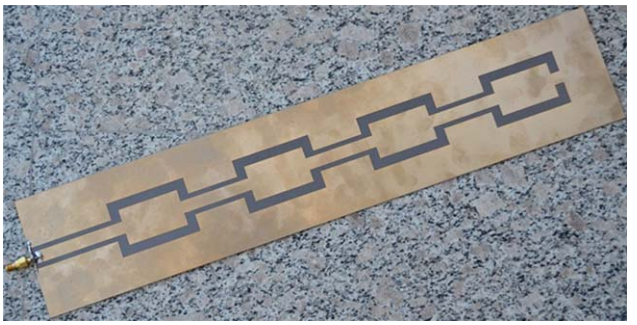

Figure 7 Photograph of the fabricated antenna prototype. [Color figure can be viewed in the online issue, which is available at wileyonlinelibrary.com]

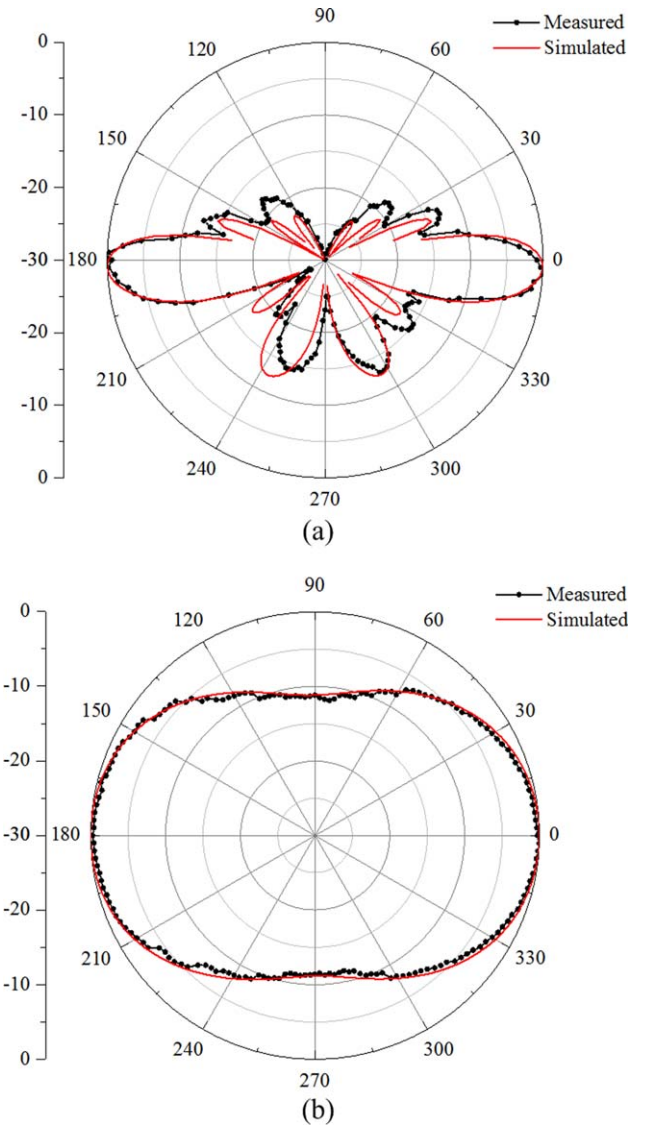

Figure 9 Measured and simulated normalized radiation patterns at 2.44 GHz: (a) *xoz* plane; (b) *yoz* plane. [Color figure can be viewed in the online issue, which is available at wileyonlinelibrary.com]

feeding length of the CPW transmission line to excite the two adjacent half-wavelength spaced elements is also half the wavelength. Therefore, no meandering on the feeding slot line is needed compared with the traditional straight slot array antenna. The antenna pattern and efficiency can be improved. A prototype for 2.4-GHz WLAN (2.4–2.48 GHz) coal mine or tunnel channel is manufactured and experimentally tested to verify our design. The measured and the simulated results agree well with each other.

ACKNOWLEDGMENTS

This work is supported by the National Basic Research Program of China under Contract 2010CB327400, in part by the National High Technology Research and Development Program of China (863 Program) under Contract 2009AA011503, the National Natural Science Foundation of China under Contract 61271135, the National Science and Technology Major Project of the Ministry of Science and Technology of China 2010ZX03007-001-01 and Qualcomm.

REFERENCES

1. H. Kobayashi and Y. Yasuoka, Slot-array antennas fed by coplanar waveguide for millimeter-wave radiation, IEEE Trans Antennas Propag 46 (1998), 800–805.
2. T.-F. Huang, S.-W. Lu, and P. Hsu, Analysis and design of coplanar waveguide-fed slot antenna array, IEEE Trans Antennas Propag 47 (1999), 1560–1565.
3. E.A. Soliman, S. Brebels, G. Vandenbosch, and E. Beyne, X-band brick wall antenna fed by CPW, Electron Lett 34 (1998), 836–838.
4. S.-Y. Chen and P. Hsu, A CPW-fed horn-shaped slot array antenna for 5-GHz WLAN access point, In: European Conference on Wireless Technology, 2004, pp. 281–284.
5. S. Sierra-Garcia and J.-J. Laurin, Study of a CPW inductively coupled slot antenna, IEEE Trans Antennas Propag 47 (1999), 58–64.
6. A. Grbic and G.V. Eleftheriades, Leaky CPW-based slot antenna arrays for millimeter-wave applications, IEEE Trans Antennas Propag 50 (2002), 1494–1504.
7. S. Chen and P. Hsu, Open-ended rampart slot array antenna fed by a CPW, IEEE Antennas Wireless Propag Lett 4 (2005), 320–322.
8. C.M. Allen, A.A. Eldek, A.Z. Elsherbeni, C.E. Smith, C.-W. Paul Huang, and K.-F. Lee, Dual tapered meander slot antenna for radar applications, IEEE Trans Antennas Propag 53 (2005), 2324–2328.
9. S.H. Kim, J.H. Choi, J.W. Baik, and Y.S. Kim, CPW-fed log-periodic dumb-bell slot antenna array, Electron Lett 42 (2006), 436–438.
10. A.U. Bhobe, C. L.Holloway, M. Piket-May, and R. Hall, Wide-band slot antennas with CPW feed lines: Hybrid and log-periodic designs, IEEE Trans Antennas Propag 52 (2004), 2545–2554.
11. S.-Y. Chen, P.-H. Wang and P. Hsu, Uniplanar log-periodic slot antenna fed by a CPW for UWB applications, IEEE Antennas Wireless Propag Lett 5 (2006), 256–259.

A COMPACT COUPLING CONTROLLABLE ELLIPTICAL FILTER BASED ON MULTILAYER LTCC

Fanyi Meng,[1] Kaixue Ma,[1] Kiat Seng Yeo,[1] Chirn Chye Boon,[1] Shanshan Xu,[1] Wei Meng Lim,[1] and Manh Anh Do[1]

VIRTUS, IC Design Centre of Excellence, School of Electrical and Electronic Engineering, Nanyang Technological University, Singapore 639798, Singapore; Corresponding author: meng.fanyi@gmail.com

Received 3 December 2012

ABSTRACT: *This paper presents a compact elliptical filter based on modified λ/4 resonators with separated electric and magnetic coupling paths. For the proposed second-order filters, transmission zero points are generated at either lower or upper stopband by controlling the relative coupling strength in the two paths of inter-stage resonators. Based on the topology and multilayer LTCC technology, a fourth-order bandpass filters operating at 5.2 GHz with a fractional bandwidth of 10% in 1.7 mm × 3 mm (0.0785λg × 0.1385λg) is designed and verified experimentally.* © 2013 Wiley Periodicals, Inc. Microwave Opt Technol Lett 55:1789–1792, 2013; View this article online at wileyonlinelibrary.com. DOI 10.1002/mop.27679

Key words: *bandpass filter; low temperature co-fired ceramic; miniaturization*

1. INTRODUCTION

Miniaturized microstrip bandpass filters (BPFs) are extensively demanded in wireless and portable communication technology due to size, cost, and fabrication advantages. Various research efforts of microstrip filter miniaturization are reported in literature, including the use of dual-mode resonators [1], multilayer structures [2], slow-wave effects [3], meandering [4], and lumped elements [5]. In general, dual-mode designs are physically compact but introduce complexity in design procedures [1]. Slow-wave approach [3] is not very practical for large fractional bandwidth designs, even though it offers excellent wideband response, and it is not always practical to realize lumped elements [5].

For the same filter order, filters based on $\lambda/4$ resonators [6,7] have more compact size compared to $\lambda/2$ resonator filters. In [7], a filter topology with two separate electric and magnetic coupling paths was proposed. By inserting K-inverters, the filter can be made much more compact with good selectivity.

In this article, a novel multilayer doublet structure containing two $\lambda/4$ resonators with electric and magnetic coupling paths in parallel is introduced. The mechanism of generating zero points is investigated and discussed by separately analyzing the two coupling paths. Based on the theoretical study, the coupling scheme is extended to a cascaded doublet that a fourth-order filter with controllable transmission zeros at both lower and upper stopband is designed and fabricated on multilayer low temperature co-fired ceramic (LTCC). Both simulation and measurement results show that the proposed filter has a good performance and compact size.

2. SECOND-ORDER FILTER REALIZATION

The proposed second-order filter is shown in Figure 1(a), consisting of two parallel coupling paths magnetic coupling path (M-path) in Figure 1(b) and electric coupling path (E-path) in Figure 1(c) on three metal layers. Layer 2 is the common ground plane. M-path is formed on layer 1 using short stub and via hole. E-path comprises of short microstrip lines (MLs) in layer 1, via from layer 1 to layer 3, and long microstrip lines (MLs) with adjacent open-end traces in layer 3. As the common ground layer physically separates M- and E-paths and negligible cross-coupling exists in between, the two paths can be controlled and analyzed separately.

Because the configurations are symmetrical, the calculated scattering matrix can be converted into admittance matrix for both M- and E-paths using

$$Y_{11}{}^{M/E} = Y_{22}{}^{M/E} = \frac{1-\left(S_{11}{}^{M/E}\right)^2+\left(S_{21}{}^{M/E}\right)^2}{\left(1-S_{11}{}^{M/E}\right)^2-\left(S_{21}{}^{M/E}\right)^2}Y_0 \quad (1)$$

$$Y_{21}{}^{M/E} = Y_{12}{}^{M/E} = \frac{-2S_{21}{}^{M/E}}{\left(1\text{-}S_{11}{}^{M/E}\right)^2-\left(S_{21}{}^{M/E}\right)^2}Y_0 \quad (2)$$

where Y_0 is the port admittance. As the two paths are in parallel, the overall admittance matrix is used to find the scattering matrix of the collective configuration in Figure 1(a) as